

Geometry-Controlled Work Extraction in a Non-Markovian Quantum Battery

Maryam Hadipour ¹ and Soroush Haseli ^{1,*}

¹*Faculty of Physics, Urmia University of Technology, Urmia, Iran*

(Dated: February 23, 2026)

We investigate the role of spatial geometry in controlling energy storage and work extraction in a non-Markovian quantum battery. The model consists of two identical two-level systems embedded in a structured waveguide environment, where one qubit acts as the charger and the other as the battery. The relative separation between the qubits introduces a geometry-dependent phase that governs collective interference effects and modulates.

Keywords: Ergotropy, Thermal bath, qubit, Coupled qubits

Introduction.— In recent years the thermodynamic effects and consequences arising from quantum evolution have emerged as a fundamental framework for the development of novel architectures for high-efficiency energy storage devices. These advances also provide the basis for the formulation and optimization of precise protocols for the control, conversion, and management of work and heat, approaches that open perspectives beyond the intrinsic limitations of classical thermodynamic processes [1–4].

Within this framework, quantum energy storage devices, commonly referred to as Quantum Batteries (QBs), have emerged in recent years as a central subject of both theoretical and experimental research. Owing to their ability to exploit uniquely quantum mechanical features, such as superposition and entanglement, these systems offer novel prospects for efficient energy storage and transfer. In realistic scenarios, any physical quantum system inevitably interacts with its surrounding environment. Consequently, investigating quantum batteries within the framework of open quantum systems is of fundamental importance. Environmental interactions lead to dissipation, decoherence, and memory effects that significantly influence charging dynamics, energy retention, and extractable work. Therefore, studying quantum batteries in the context of open quantum systems is essential for assessing their practical performance and operational stability [5].

Consequently, they have been extensively investigated and systematically analyzed in the contemporary literature [4, 6–14]. Quantum batteries have been theoretically and experimentally investigated across a broad range of physical realizations. Proposed schemes include spin-chain models [15–18], atomic ensembles coupled to optical cavities [19–23], and superconducting systems [24–26]. These diverse approaches rely on different interaction mechanisms and control techniques, thereby enabling the exploration of multiple strategies for microscopic energy storage and controlled energy transfer within quantum regimes.

Although the enhancement of charging power in

quantum batteries, together with its favorable scaling with system size [27–29], presents an encouraging prospect, practical implementation remains significantly challenged by the phenomenon of self-discharge induced by environmental interactions. Energy dissipation and the degradation of quantum coherence, arising from unavoidable coupling to the surroundings, can substantially constrain the long-term performance and stability of these devices.

To mitigate these limitations, several sophisticated strategies have been proposed. These include the deliberate exploitation of quantum coherence in conjunction with disordered local fields [30], the storage of energy in decoherence-resistant dark states [31, 32], and the investigation of non-Markovian dynamical effects as a means of alleviating dissipative losses [33–36]. Collectively, these approaches seek to extend the operational lifetime over which quantum batteries can reliably retain stored energy without significant performance degradation. Furthermore, considerable research efforts have been devoted to elucidating the possible connection between quantum correlations and the charging efficiency of quantum batteries [37]. Despite these extensive investigations, a comprehensive and universally accepted relationship has yet to be established.

In this work, we investigate the role of the relative geometry between the charger and the quantum battery in a structured environment. In particular, we examine how the spatial separation between the two qubits and the associated geometric phase k_0d influence the energy transfer process, charging dynamics and the amount of the extractable work of the battery through their control over collective interference and the spectral structure of the environment. Within this framework, we demonstrate that the system geometry not only regulates the effective coupling strength between the charger and the environment, but also, through the engineering of bright and dark collective channels, can suppress or enhance decay processes and energy backflow. As a result, the thermodynamic performance of the battery, including charging time, charging power, and maximum ergotropy, becomes directly governed by the geometric distance parameter. Furthermore, our analysis reveals that in the presence of environmental memory (non-Markovian effects), the system geometry can give rise to distinct regions in param-

* soroush.haseli@uut.ac.ir

eter space where the revival of extractable work occurs. In this sense, geometry emerges as a fundamental control resource, enabling the active engineering and optimization of quantum battery performance.

Figures of merit.— In this section, we present the thermodynamic framework employed to analyze quantum batteries. The system under consideration is a quantum battery characterized by the Hamiltonian H_B , with its state described by the density operator ρ_B . This quantum state can be expressed through its spectral decomposition in terms of its eigenvalues r_j and corresponding eigenvectors $|r_j\rangle$

$$\rho_B = \sum_j r_j |r_j\rangle\langle r_j| \quad r_j \geq r_{j+1}, \quad (1)$$

where the eigenvalues are non-negative and satisfy the normalization condition. Likewise, the Hamiltonian H_B admits a spectral decomposition in terms of its energy eigenvalues \mathcal{E}_i and eigenstates $|\mathcal{E}_i\rangle$

$$H_B = \sum_i \mathcal{E}_i |\mathcal{E}_i\rangle\langle \mathcal{E}_i| \quad \mathcal{E}_i \leq \mathcal{E}_{i+1}. \quad (2)$$

From an energetic perspective, the energy stored in the battery is given by the expectation value of the Hamiltonian with respect to the state ρ_B , representing the total energy content of the system

$$E_B = \langle H_B \rangle_{\rho_B} = \text{tr}(\rho_B H_B). \quad (3)$$

However, not all of this energy is necessarily extractable as useful work. To quantify the portion that can be converted into work, the concept of ergotropy is introduced. Ergotropy specifies the maximum amount of work that can be extracted from the system via cyclic unitary operations and is determined by comparing the energy of the given state with that of its corresponding passive state σ_ρ , from which no further work can be extracted through unitary operations. So, the ergotropy is given by [38]

$$\mathcal{W} = \text{tr}(\rho_B H_B) - \text{tr}(\sigma_\rho H_B), \quad (4)$$

where the passive state defined as a diagonal state in the energy eigenbasis that possesses no population inversion and can be written as

$$\sigma_\rho = \sum_i r_i |\mathcal{E}_i\rangle\langle \mathcal{E}_i|, \quad (5)$$

in above the populations r_i are ordered in a non-increasing manner with respect to the increasing energy eigenvalues \mathcal{E}_i . One of the most significant and appealing features of quantum batteries is their capability for rapid charging, a property that is commonly assessed in terms of either instantaneous power or average power. In particular, the average power provides a simple and practical figure of merit and is defined as the energy stored in the battery over a given charging interval divided by the duration of the energy-storage process. In other words,

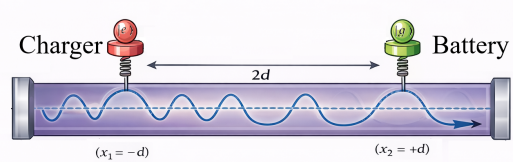


FIG. 1. Schematic of the physical model: two identical two-level systems separated by a distance $2d$ inside a mirror-terminated one-dimensional waveguide. Qubit 1 acts as the charger (initially excited) and qubit 2 as the quantum battery (initially in the ground state). The spatial phase $k_0 d$ controls collective interference and energy transfer dynamics.

it quantifies the rate at which energy is accumulated in the system: $\mathcal{P} = E_B/t$. Our main goal in this paper is to study the geometry-dependent charging and work extraction dynamics of a quantum battery. To this end, we consider a model in which the geometric configuration of the charger and the battery is explicitly incorporated as a fundamental control parameter. In the following section, we introduce the theoretical framework and present the detailed description of the model.

Physical model.— We consider a composite quantum system consisting of two identical two-level systems (TLSs) positioned at $x_1 = -d$ and $x_2 = +d$, respectively. Within the quantum battery paradigm, one TLS is designated as the charger, while the other functions as the battery. This physical setup is equivalent to two qubits placed inside a mirror-terminated one-dimensional waveguide of length L , where the boundary conditions discretize the electromagnetic field into a uniformly spaced ladder of standing-wave modes characterized by $k_n = n\pi/L$. The mode spacing is $\delta\omega = \pi v/L$, with v denoting the group velocity. Such discretization introduces a natural environmental timescale associated with field rephasing, which plays a crucial role in the energy backflow and work revival phenomena observed in the quantum battery. We set $\hbar = 1$ and work within the dipole and rotating-wave approximations. The total Hamiltonian of the system can be written as

$$H = H_S + H_B + H_I, \quad (6)$$

where H_S describes the free Hamiltonian of the two qubits (charger and battery), H_B represents the discrete bosonic modes of the structured waveguide environment, and H_I accounts for the interaction between the qubits and the environmental modes. The system Hamiltonian reads [39]

$$H_S = \omega_0(\sigma_1^+ \sigma_1^- + \sigma_2^+ \sigma_2^-) + J(\sigma_1^+ \sigma_2^- + \sigma_1^- \sigma_2^+), \quad (7)$$

where ω_0 is the transition frequency of the two-level systems. The parameter J represents the coherent dipole-dipole interaction [40]. In the quantum battery interpretation adopted here, qubit 1 acts as the charger, while qubit 2 represents the battery. The operators σ_j^\pm denote the raising and lowering operators of the j -th qubit. The

bath Hamiltonian is given by

$$H_B = \sum_k \omega_k a_k^\dagger a_k, \quad (8)$$

with a_k^\dagger (a_k) being the creation (annihilation) operator of the k -th standing-wave mode of the waveguide. The interaction Hamiltonian, within the rotating-wave approximation, takes the form

$$H_{SB} = \sum_k \left[g_k^{(1)} \sigma_1^- a_k^\dagger + g_k^{(2)} \sigma_2^- a_k^\dagger + h.c. \right]. \quad (9)$$

The model is schematically illustrated in Fig. 1. The influence of geometry is encoded in the coupling amplitudes $g_k^{(j)} = g_k e^{ikx_j}$, with x_j representing the location of the j -th qubit [41–44]. The resulting phase difference between the qubits generates interference in the collective channels, enabling controlled modulation of both charging dynamics and work extraction. Since the interaction of the qubits predominantly occurs with modes near their transition frequency ω_0 , we simplify the analytical treatment by approximating the wave number in the position-dependent phase terms as $k \approx k_0 = \omega_0/v = 2\pi/\lambda_0$, while retaining the full dispersion relation ω_k elsewhere in the Hamiltonian. Here, λ_0 denotes the resonant wavelength associated with the qubit transition frequency. Consequently, the position-dependent coupling coefficients can be expressed as

$$g_k^{(1)} \simeq g_k e^{+ik_0 d}, \quad g_k^{(2)} \simeq g_k e^{-ik_0 d}. \quad (10)$$

In this form, the geometric dependence of the system is explicitly encoded in the phase factor $k_0 d$. This phase plays a crucial role in controlling the interference between collective interaction channels and, in turn, determines the energy transfer dynamics and the amount of extractable work in the quantum battery. This approximation introduces a negligible error for physically relevant parameter regimes, remaining well below typical numerical thresholds. Consequently, it can be regarded as a well-controlled and reliable procedure. Widely adopted in studies of collective emission and waveguide quantum electrodynamics, this substitution preserves all geometry-induced interference effects while substantially simplifying the mathematical treatment. As a result, it enables closed-form analytical solutions in both discrete and continuous reservoir regimes [45, 46].

Collective Modes: Symmetric–Antisymmetric Decomposition and Interference.—Importantly, the total number of excitations in the system is conserved. As a result, the dynamics can be restricted to the single-excitation subspace, allowing for an exact and significantly simplified treatment of the energy exchange between the charger, the battery, and the structured environment. The total state of the system within the single-excitation sector can be written as

$$|\Psi(t)\rangle = \alpha_1(t) |eg, \{0\}\rangle + \alpha_2(t) |ge, \{0\}\rangle + \sum_k \beta_k(t) |gg\rangle \otimes |1_k\rangle, \quad (11)$$

where $|e\rangle_j$ and $|g\rangle_j$ denote the excited and ground states of the j -th two-level system, respectively. The states $|eg\rangle$ and $|ge\rangle$ represent configurations in which the excitation resides in the charger or in the battery, while the other qubit remains in its ground state. The state $|1_k\rangle$ corresponds to a single excitation in the k -th environmental mode, with both qubits in the ground state. This decomposition explicitly captures the energy exchange pathways between the charger, the battery, and the structured reservoir, and provides the basis for an exact treatment of the dynamics within the single-excitation manifold.

To facilitate the analysis of the system dynamics, it is advantageous to introduce the collective symmetric and antisymmetric basis. In this representation, the collective amplitudes are defined as $s(t) = (\alpha_1(t) + \alpha_2(t))/\sqrt{2}$ and $a(t) = (\alpha_1(t) - \alpha_2(t))/\sqrt{2}$ which correspond to the symmetric $|S\rangle = (|eg\rangle + |ge\rangle)/\sqrt{2}$ and antisymmetric $|A\rangle = (|eg\rangle - |ge\rangle)/\sqrt{2}$ collective states. This collective representation diagonalizes the coherent exchange interaction between the charger and the battery, thereby simplifying the mathematical structure of the problem. Within this basis, and under the near-resonant approximation, the system–environment interaction Hamiltonian can be compactly expressed as

$$H_{SB} = \sum_k \sqrt{2} g_k \left[\cos(k_0 d) \sigma_S^+ + i \sin(k_0 d) \sigma_A^+ \right] b_k + \text{H.c.}, \quad (12)$$

where the collective raising operators are defined as $\sigma_{S,A}^+ = (\sigma_1^+ \pm \sigma_2^+)/\sqrt{2}$. This form of the interaction Hamiltonian explicitly reveals how the geometric dependence enters the dynamics through the factors $\cos(k_0 d)$ and $\sin(k_0 d)$, which determine the effective coupling strength of the symmetric and antisymmetric collective channels to the environment. This expression shows that the symmetric and antisymmetric collective channels interact independently with the reservoir, and that the coupling strength of each channel depends explicitly on the interqubit separation. The geometric dependence enters the dynamics through the factors $\cos(k_0 d)$ and $\sin(k_0 d)$, such that the symmetric channel couples to the environment with amplitude proportional to $\cos(k_0 d)$, while the antisymmetric channel couples with amplitude proportional to $\sin(k_0 d)$.

For specific separations $d = n\lambda_0/2$, where $\sin(k_0 d) = 0$, the antisymmetric channel becomes completely decoupled from the reservoir and thus forms a geometry-protected dark state, whereas the symmetric channel remains coupled to the bath. Conversely, for separations $d = (2n + 1)\lambda_0/4$, where $\cos(k_0 d) = 0$, the symmetric channel becomes fully decoupled and forms the dark

state, while the antisymmetric channel continues to interact with the environment.

The full details of the dynamical analysis are presented in the Appendix.A, where the derivation of the equations of motion, underlying assumptions, and intermediate analytical steps are provided in a systematic and comprehensive manner. Taking the partial trace over the environmental and charger degrees of freedom in Eq. (11), the reduced density matrix describing the quantum battery is obtained as follows

$$\rho_B(t) = \begin{pmatrix} P_B(t) & 0 \\ 0 & 1 - P_B(t) \end{pmatrix}, \quad (13)$$

where $P_B(t) = |\alpha_2(t)|^2$ denotes the excitation probability of the quantum battery. The internal energy of the quantum battery is then given by

$$E_B(t) = \omega_0 |\alpha_2(t)|^2. \quad (14)$$

By employing the definition of ergotropy given in Eq. (1), and taking into account the density matrix and the Hamiltonian of the battery, the ergotropy can be expressed in the following form

$$\mathcal{W}(t) = (2|\alpha_2(t)|^2 - 1)\Theta(|\alpha_2(t)|^2 - \frac{1}{2}), \quad (15)$$

where $\Theta(\cdot)$ is the Heaviside function. The charging power of the quantum battery for this model can also be expressed as follows

$$\mathcal{P}_B(t) = 2\omega_0 \Re[\alpha_2^*(t) \dot{\alpha}_2(t)]. \quad (16)$$

The charging performance of the quantum battery can be comprehensively characterized by its optimal energetic figures of merit. In particular, the maximum stored energy, ΔE_B^{\max} , and the maximum ergotropy, \mathcal{W}^{\max} , quantify the ultimate energy-storage capacity and work-extraction capability of the battery. These quantities are defined as

$$\Delta E_B^{\max} = \max_{\tau} [\Delta E_B(\tau)], \quad \mathcal{W}^{\max} = \max_{\tau} [\mathcal{W}(\tau)], \quad (17)$$

where the optimization is performed over the charging time τ .

In addition, the maximal charging power plays a crucial role in assessing the dynamical performance of the system. It is defined as

$$P^{\max} = \max_{\tau} [P(\tau)], \quad (18)$$

which determines the highest achievable rate of energy transfer during the charging process.

For optimal operation of the quantum battery, both ΔE_B^{\max} and \mathcal{W}^{\max} should attain large values, ensuring substantial energy storage and maximal extractable work, while a large P^{\max} guarantees rapid charging. Together, these quantities provide a comprehensive evaluation of the battery's energetic and dynamical performance.

In Fig. 2(a), we present the time-geometry plot of the internal energy variation of the quantum battery, $\Delta E_B(t)$, for the parameters $g = 0.05\omega_0$, $J = -0.005\omega_0$, and $\lambda/g = 0.02$. The small value of λ places the system in the weak-dissipation, non-Markovian regime, where reservoir memory effects significantly influence the dynamics. The figure reveals a pronounced modulation of the charging process as a function of the geometric parameter d/λ_0 . The vertical band structure indicates that the efficiency of energy transfer from the charger to the battery is strongly governed by the relative spatial phase k_0d . This behavior originates from the geometry-dependent collective decay rates, $\Gamma_S \propto \cos^2(k_0d)$ and $\Gamma_A \propto \sin^2(k_0d)$, which determine the effective coupling of the symmetric and antisymmetric collective channels to the structured reservoir. Consequently, constructive interference enhances energy transfer at specific separations, while destructive interference suppresses it, giving rise to geometry-induced dark configurations in which charging is strongly inhibited. The oscillatory structures along the temporal axis reflect coherent energy exchange between the charger and the battery that persists due to the long reservoir correlation time ($\lambda \ll g$). The appearance of revival-like features signals partial information and energy backflow from the reservoir, which is a characteristic signature of non-Markovian dynamics. Notably, both the maximum stored energy and the optimal charging time depend sensitively on the inter-qubit separation. Overall, the results demonstrate that in a structured environment the spatial geometry of the system acts as an effective control parameter for tuning the charging efficiency, dynamical stability, and the interplay between coherent exchange and dissipation. In particular, optimal charging occurs at separations where collective bright-state coupling is maximized, whereas dark-state configurations suppress energy transfer despite finite system-environment interaction.

Fig. 2(b), depicts the time-geometry dependence of the battery ergotropy under the same parameter regime as Fig. 2(a). In contrast to internal energy, ergotropy quantifies the extractable portion of the stored energy and therefore provides a direct measure of the battery's operational performance. The map reveals that extractable work is highly selective in both time and geometry. While internal energy may accumulate over extended parameter regions, ergotropy emerges only in well-defined localized domains. This indicates that energy storage alone is insufficient for work extraction; the battery must reach a sufficiently non-passive state. The strong modulation along the geometric axis demonstrates that the relative spatial separation between charger and battery governs the efficiency of work generation. Constructive interference enhances collective coupling and promotes effective energy transfer, leading to pronounced ergotropy peaks. Conversely, destructive interference suppresses coherent exchange, resulting in extended regions where extractable work remains negligible. The appearance of isolated bright regions in time reflects the

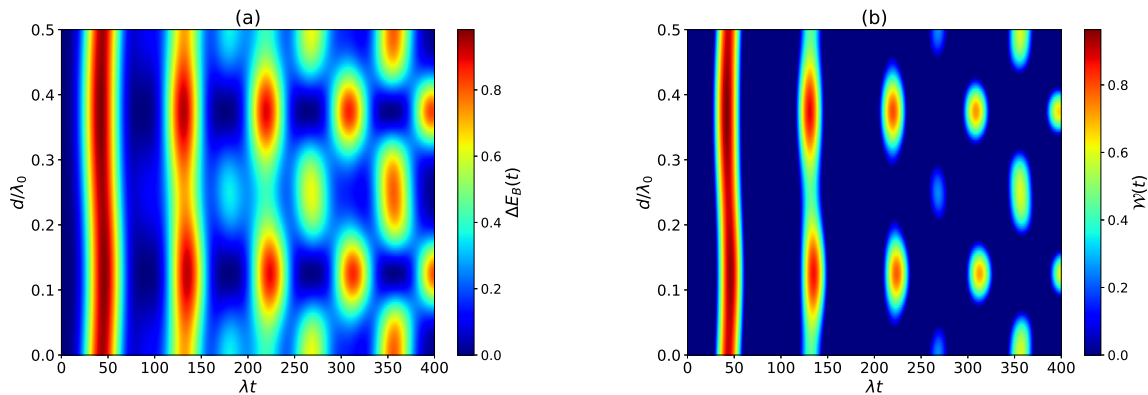


FIG. 2. Time-geometry plot of (a) the internal energy change $\Delta E_B(t)$ and (b) the ergotropy $\mathcal{W}(t)$. The battery is initially in its ground state and the charger excited. The parameters are $\omega_0 = 1$, $g = 0.05 \omega_0$, $J = -0.005 \omega_0$, and $\lambda/g = 0.02$.

interplay between coherent dynamics and environmental memory. In the weak-dissipation regime considered here, partial information backflow enables transient revivals of extractable work, producing discrete activation windows rather than continuous charging. Overall, the figure demonstrates that geometry functions as a fundamental control parameter for the thermodynamic activity of the quantum battery, determining not only how energy is stored but whether and when it becomes operationally useful.

Fig. 3(a) shows the internal energy change of the quantum battery, $\Delta E_B(t)$, for three representative geometric configurations defined by $\sin(k_0 d) = 0$, $\cos(k_0 d) = 0$, and $\sin(2k_0 d) = 1$. The parameters $\omega_0 = 1$, $g = 0.05 \omega_0$, $J = -0.005 \omega_0$, and $\lambda/g = 0.02$ correspond to a weak-dissipation, strongly non-Markovian regime, with the initial state $|eg\rangle$. The purely symmetric ($\sin(k_0 d) = 0$) and purely antisymmetric ($\cos(k_0 d) = 0$) configurations yield nearly identical charging dynamics. In both cases, one collective channel is completely dark, while the other remains fully coupled to the structured reservoir. Since the initial state contains equal symmetric and antisymmetric components, eliminating either channel effectively reduces the dynamics to a single active collective mode with comparable effective coupling strength. As a result, the internal energy evolution is symmetric under exchange of the two channels, leading to identical charging behavior. In contrast, the mixed configuration defined by $\sin(2k_0 d) = 1$ allows both collective channels to couple simultaneously and with equal strength. In this regime no dark-state protection occurs, and the symmetric and antisymmetric contributions jointly enhance the energy exchange between charger and battery. This results in larger oscillation amplitudes and improved charging performance. The long-lived oscillations observed in all cases arise from the small reservoir spectral width ($\lambda/g \ll 1$), which induces strong memory effects and enables repeated energy exchange between the system and the structured environment. Overall, the figure demonstrates that maximal charging is achieved when both col-

lective channels contribute coherently, whereas single-channel (bright-only) configurations yield reduced performance despite full coupling strength.

Fig. 3(b) shows the time evolution of the battery ergotropy for the same geometric configurations considered in Fig. 3(a). Unlike the internal energy, the ergotropy quantifies only the extractable work stored in the battery and therefore provides a more stringent indicator of charging performance. The purely symmetric and purely antisymmetric configurations exhibit nearly identical ergotropy dynamics, consistent with the fact that in both cases only one collective channel remains active while the other is dark. Since the initial state contains equal contributions from the two collective components, suppressing either channel leads to equivalent effective dynamics and thus identical work extraction behavior. In contrast, the mixed configuration displays significantly enhanced ergotropy and more pronounced revival peaks. When both collective channels contribute simultaneously, coherent interference strengthens the effective energy transfer and increases the population inversion of the battery, thereby maximizing the extractable work. The repeated appearance of ergotropy peaks reflects the non-Markovian character of the reservoir, which enables recurrent energy exchange between the system and its environment. Overall, the figure demonstrates that optimal work extraction is achieved when symmetric and antisymmetric channels act jointly, highlighting the crucial role of geometry in enhancing quantum battery performance.

Fig. 4 summarizes the geometry spectral width dependence of the quantum battery performance. Panel (a) shows the maximum internal energy ΔE_B^{\max} , panel (b) the maximum charging power \mathcal{P}_B^{\max} , and panel (c) the maximum ergotropy \mathcal{W}_B^{\max} as functions of the geometric parameter d/λ_0 and the normalized reservoir spectral width λ/g . In all three panels, the battery performance is strongly enhanced in the small-spectral width regime ($\lambda/g \ll 1$), where reservoir memory effects are significant. As λ/g increases, both the maximum stored energy and the extractable work decrease monotonically,

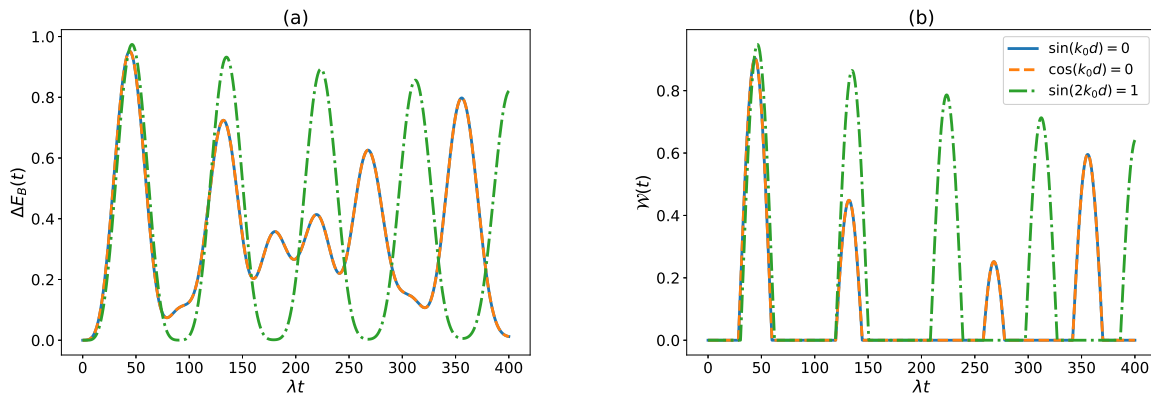


FIG. 3. (a) the internal energy change $\Delta E_B(t)$ and (b) the ergotropy $\mathcal{W}(t)$, as function of λt for different values of geometry parameter. The battery is initially in its ground state and the charger excited. The parameters are $g = 0.05 \omega_0$, $J = -0.005 \omega_0$, and $\lambda/g = 0.02$.

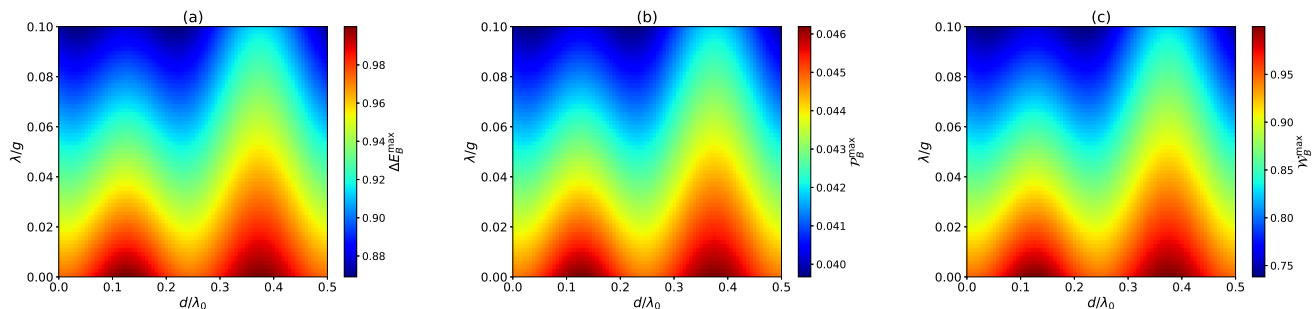


FIG. 4. Geometry and spectral width dependence of quantum battery performance for $J = -0.005 \omega_0$. (a) Maximum internal energy ΔE_B^{\max} , (b) maximum charging power \mathcal{P}_B^{\max} , and (c) maximum ergotropy \mathcal{W}_B^{\max} as functions of the geometric parameter d/λ_0 and normalized reservoir spectral width λ/g . Optimal performance occurs at small λ/g and geometries supporting constructive collective interference.

indicating the progressive suppression of coherent energy exchange in the Markovian limit. This behavior reflects the reduction of information backflow and the transition toward irreversible dissipation. Along the geometric axis, a clear periodic modulation appears in all quantities. The maxima occur at specific separations corresponding to constructive collective interference, where both symmetric and antisymmetric channels contribute effectively to the dynamics. In contrast, reduced performance is observed near configurations associated with partial destructive interference. Importantly, the locations of optimal geometry are consistent across internal energy, charging power, and ergotropy, demonstrating that geometry acts as a universal control parameter for both energy storage and work extraction. While ΔE_B^{\max} and \mathcal{W}_B^{\max} exhibit similar spatial structures, the charging power map shows a sharper sensitivity to spectral width, indicating that fast charging is more strongly affected by reservoir-induced decoherence than the total stored energy. Overall, Fig. 4 demonstrates that optimal quantum battery performance is achieved in the combined regime of strong collective interference (appropriate geometry) and long reservoir memory (small λ/g), highlighting the cooperative role of spatial phase engineering and non-

Markovian dynamics.

I. CONCLUSION

In this work, we have demonstrated that spatial geometry constitutes a fundamental control parameter for the operation of a quantum battery embedded in a structured environment. By engineering the relative separation between the charger and the battery, the collective interference between symmetric and antisymmetric channels can be selectively enhanced or suppressed, thereby directly modulating the effective system-reservoir interaction.

Our results show that optimal charging and maximal work extraction are achieved when both collective pathways contribute coherently to the dynamics. In contrast, geometries that induce dark-state formation partially decouple the system from the reservoir and limit the accessible energy and ergotropy. The presence of reservoir memory further amplifies these interference effects, enabling persistent oscillatory energy exchange and revival of extractable work in the non-Markovian regime.

The combined analysis of internal energy, charging power, and ergotropy reveals that geometry and environmental spectral width jointly determine the operational performance of the battery. While reduced spectral width enhances coherent energy exchange and improves storage capability, constructive collective interference is essential for maximizing extractable work.

Overall, our study establishes geometry as a powerful and experimentally accessible resource for engineering quantum battery performance. The ability to tune charging dynamics through spatial phase control opens new avenues for designing interference-based quantum energy devices in structured photonic environments.

-
- [1] J. Goold, M. Huber, A. Riera, L. del Rio and P. J. Skrzypczyk, The role of quantum information in thermodynamics. *Phys. A: Math. Theor.* 49, 143001 (2016).
- [2] R. Kosloff, Quantum thermodynamics: a dynamical viewpoint. *Entropy* 15, 2100 (2013).
- [3] S. Vinjanampathy and J. Anders, Quantum thermodynamics. *Contemp. Phys.* 57, 1–35 (2015).
- [4] D. Gelbwaser-Klimovsky, W. Niedenzu and G. Kurizki, Thermodynamics of quantum systems under dynamical control. *Adv. Atom. Mol. Opt. Phys.* 64, 329 (2015).
- [5] H.-P. Breuer and F. Petruccione, *The Theory of Open Quantum Systems* (Oxford University Press, Oxford, 2007).
- [6] R. Alicki and M. Fannes, Entanglement boost for extractable work from ensembles of quantum batteries, *Phys. Rev. E* 87, 042123 (2013).
- [7] A. Crescente, M. Carrega, M. Sassetti, and D. Ferraro, Ultrafast charging in a two-photon Dicke quantum battery, *Phys. Rev. B* 102, 245407 (2020).
- [8] F.-Q. Dou and F.-M. Yang, Superconducting transmon qubitresonator quantum battery, *Phys. Rev. A* 107, 023725 (2023).
- [9] F. Campaioli, S. Gherardini, J. Q. Quach, M. Polini, and G. M. Andolina, Colloquium: Quantum batteries, *Rev. Mod. Phys.* 96, 031001 (2024).
- [10] F. T. Tabesh, F. H. Kamin, S. Salimi, Environment-mediated charging process of quantum batteries, *Phys. Rev. A* 102 (5), 052223 (2020).
- [11] F. H. Kamin, F. T. Tabesh, S. Salimi, F. Kheirandish, A. C. Santos, Non-Markovian effects on charging and self-discharging process of quantum batteries, *New Journal of Physics* 22 (8), 083007 (2020).
- [12] F. H. Kamin, S. Salimi, M. B. Arjmandi, Steady-state charging of quantum batteries via dissipative ancillas, *Phys. Rev. A* 109 (2), 022226 (2024).
- [13] A. Shokri, E. Faizi, M. B. Arjmandi, Entanglement-assisted charging of quantum batteries within optomechanical framework, *Phys. Rev. E* 111 (6), 064117 (2025).
- [14] B. Mojaveri, R. Jafarzadeh Bahrbeig, M. A. Fasihi, Extracting ergotropy from nonequilibrium steady states of an XXZ spin-chain quantum battery, *Phys. Rev. A* 109 (4), 042619 (2024).
- [15] T. P. Le, J. Levinsen, K. Modi, M. M. Parish, F. A. Pollock, Spin-chain model of a many-body quantum battery, *Phys. Rev. A*, 97(2), 022106, (2018).
- [16] Y. Yao, X. Q. Shao, Optimal charging of open spin-chain quantum batteries via homodyne-based feedback control, *Phys. Rev. E*, 106(1), 014138, (2022).
- [17] D. Rossini, G. M. Andolina, M. Polini, Many-body localized quantum batteries, *Phys. Rev. B*, 100(11), 115142, (2019).
- [18] M. B. Arjmandi, H. Mohammadi, A. Saguia, M. S. Sarandy, A. C. Santos, Localization effects in disordered quantum batteries, *Phys. Rev. E*, 108(6), 064106, (2023).
- [19] G. M. Andolina, M. Keck, A. Mari, M. Campisi, V. Giovannetti, M. Polini, Extractable work, the role of correlations, and asymptotic freedom in quantum batteries, *Phys. Rev. L*, 122(4), 047702, (2019).
- [20] M. B. Arjmandi, A. Shokri, E. Faizi, H. Mohammadi, Performance of quantum batteries with correlated and uncorrelated chargers, *Phys. Rev. A*, 106(6), 062609, (2022).
- [21] A. Crescente, M. Carrega, M. Sassetti, D. Ferraro, Ultrafast charging in a two-photon Dicke quantum battery, *Phys. Rev. B*, 102(24), 245407, (2020).
- [22] D. L. Yang, F. M. Yang, F. Q. Dou, Three-level Dicke quantum battery, *Phys. Rev. B*, 109(23), 235432, (2024).
- [23] W. Zhang, S. Wang, C. Wu, G. Wang, Quantum battery based on dipole-dipole interaction and external driving field, *Phys. Rev. E*, 107(5), 054125, (2023).
- [24] C. K. Hu, J. Qiu, P. J. Souza, J. Yuan, Y. Zhou, L. Zhang, D. Yu, Optimal charging of a superconducting quantum battery, *Quantum Science and Technology*, 7(4), 045018, (2022).
- [25] F. Q. Dou, F. M. Yang, Superconducting transmon qubitresonator quantum battery, *Phys. Rev. A*, 107(2), 023725, (2023).
- [26] F. Q. Dou, Y. J. Wang, J. A. Sun, Highly efficient charging and discharging of three-level quantum batteries through shortcuts to adiabaticity, *Frontiers of Physics*, 17, 1-9, (2022).
- [27] F. C. Binder, S. Vinjanampathy, K. Modi, J. Goold, Quantacell: powerful charging of quantum batteries, *New Journal of Physics*, 17(7), 075015, (2015).
- [28] F. Campaioli, F. A. Pollock, F. C. Binder, L. C'eleri, J. Goold, S. Vinjanampathy, K. Modi, Enhancing the charging power of quantum batteries, *Phys. Rev. L*, 118(15), 150601, (2017).
- [29] S. Julia-Farre, T. Salamon, A. Riera, M. N. Bera, M. Lewenstein, Bounds on the capacity and power of quantum batteries, *Phys. Rev. R*, 2(2), 023113, (2020).
- [30] M. B. Arjmandi, H. Mohammadi, A. C. Santos, Enhancing selfdischarging process with disordered quantum batteries, *Phys. Rev. E*, 105(5), 054115, (2022).
- [31] J. Q. Quach, W. J. Munro, Using dark states to charge and stabilize open quantum batteries, *Physical Review Applied*, 14(2), 024092, (2020).
- [32] J. Liu, D. Segal, G. Hanna, Loss-free excitonic quantum battery, *The Journal of Physical Chemistry C*, 123(30), 18303-18314, (2019).
- [33] F. H. Kamin, F. T. Tabesh, S. Salimi, F. Kheirandish, A. C. Santos, Non-Markovian effects on charging and self-discharging process of quantum batteries, *New Journal of Physics*, 22(8), 083007, (2020).

- [34] D. Morrone, M. A. Rossi, A. Smirne, M. G. Genoni, Charging a quantum battery in a non-Markovian environment: a collisional model approach, *Quantum Science and Technology*, 8(3), 035007, (2023).
- [35] M. Hadipour, S. Haseli, H. Dolatkhah, M. Rashidi, Study the charging process of moving quantum batteries inside cavity, *Scientific Reports* 13 (1), 10672 (2023).
- [36] M. Hadipour, S. Haseli, D. Wang, S. Haddadi, Proposed Scheme for a Cavity-Based Quantum Battery, *Advanced Quantum Technologies* 7 (11), 2400115 (2024).
- [37] F. H. Kamin, F. T. Tabesh, S. Salimi, and A. C. Santos, Entanglement, coherence, and charging process of quantum batteries, *Phys. Rev. E*, 102, 052109, (2020).
- [38] A. E. Allahverdyan, R. Balian, T. M. Nieuwenhuizen, Maximal work extraction from finite quantum systems, *Europhysics Letters*, 67(4), 565, (2004).
- [39] M. Hatifi, Geometry-controlled freezing and revival of Bell nonlocality through environmental memory, *Phys. Rev. A* 113, 022204 (2026)
- [40] A. M. Kaufman, B. J. Lester, M. Foss-Feig, M. L. Wall, A. M. Rey, and C. A. Regal, *Nature* 527, 208 (2015).
- [41] V. Bužek, G. Drobný, M. G. Kim, M. Havukainen, and P. L. Knight, *Physical Review A* 60, 582 (1999).
- [42] J. P. Hansen and K. Tywniuk, *Physical Review A* 108, 053707 (2023).
- [43] J.-T. Shen and S. Fan, *Physical Review Letters* 98, 153003 (2007).
- [44] L. Zhou, Z. R. Gong, Y.-x. Liu, C. P. Sun, and F. Nori, *Physical Review Letters* 101, 100501 (2008).
- [45] R. H. Lehberg, *Physical Review A* 2, 883 (1970).
- [46] M. O. Scully and M. S. Zubairy, *Quantum Optics*, 1st ed. (Cambridge University Press, 1997).

Appendix A: Exact Single-Excitation Dynamics in a Lorentzian Reservoir

In this model, we assume that the quantum battery is initially empty, while the charger is prepared in its excited state. This corresponds to choosing the initial state with the conditions $\alpha_1(0) = 1, \alpha_2(0) = 0$ and $\beta_k(0) = 0$ in Eq. (11). By substituting the total state of the system at time t , together with the total Hamiltonian, into the Schrödinger equation, one obtains the following set of coupled differential equations

$$\dot{\alpha}_1(t) = -i\omega_0\alpha_1(t) - iJ\alpha_2(t) - i\sum_k g_k^{(1)}\beta_k(t), \quad (\text{A1})$$

$$\dot{\alpha}_2(t) = -i\omega_0\alpha_2(t) - iJ\alpha_1(t) - i\sum_k g_k^{(2)}\beta_k(t), \quad (\text{A2})$$

$$\dot{\beta}_k(t) = -i\omega_k\beta_k(t) - i\left[g_k^{(1)*}\alpha_1(t) + g_k^{(2)*}\alpha_2(t)\right]. \quad (\text{A3})$$

Solving Eq. (A3) with $\beta_k(0) = 0$ yields the formal bath amplitude

$$\beta_k(t) = -i\int_0^t d\tau e^{-i\omega_k(t-\tau)}\left[g_k^{(1)*}\alpha_1(\tau) + g_k^{(2)*}\alpha_2(\tau)\right]. \quad (\text{A4})$$

Substituting (A4) into (A1)–(A2) eliminates the bath and produces memory integrals. Using the standard

phase approximation for spatially separated emitters,

$$g_k^{(1)} \simeq g_k e^{+ik_0d}, \quad g_k^{(2)} \simeq g_k e^{-ik_0d}, \quad (\text{A5})$$

one obtains the integro-differential system

$$\begin{aligned} \dot{\alpha}_1(t) &= -i\omega_0\alpha_1(t) - iJ\alpha_2(t) \\ &\quad - \int_0^t d\tau K(t-\tau)\left[\alpha_1(\tau) + e^{+i2k_0d}\alpha_2(\tau)\right] \end{aligned} \quad (\text{A6})$$

$$\begin{aligned} \dot{\alpha}_2(t) &= -i\omega_0\alpha_2(t) - iJ\alpha_1(t) \\ &\quad - \int_0^t d\tau K(t-\tau)\left[\alpha_2(\tau) + e^{-i2k_0d}\alpha_1(\tau)\right] \end{aligned} \quad (\text{A7})$$

where the bath correlation kernel is

$$K(t) \equiv \int_0^\infty d\omega J(\omega) e^{-i\omega t}, \quad (t \geq 0). \quad (\text{A8})$$

By considering the collective amplitudes defined in the main text and using $e^{\pm i2k_0d} = \cos(2k_0d) \pm i\sin(2k_0d)$, the above integro-differential equations can be rewritten in the following form

$$\begin{aligned} \dot{s}(t) &= -i(\omega_0 + J)s(t) \\ &\quad - \int_0^t d\tau K(t-\tau)\zeta(\tau), \end{aligned} \quad (\text{A9})$$

$$\begin{aligned} \dot{a}(t) &= -i(\omega_0 - J)a(t) \\ &\quad - \int_0^t d\tau K(t-\tau)\xi(\tau), \end{aligned} \quad (\text{A10})$$

where $\zeta(\tau) = \left[2\cos^2(k_0d)s(\tau) + i\sin(2k_0d)a(\tau)\right]$ and $\xi(\tau) = \left[2\sin^2(k_0d)a(\tau) - i\sin(2k_0d)s(\tau)\right]$. We now assume a Lorentzian spectral density centered at ω_0 ,

$$J_L(\omega) = \frac{\gamma\lambda^2}{(\omega - \omega_0)^2 + \lambda^2}, \quad (\text{A11})$$

with coupling scale γ and linewidth λ (memory time $\tau_M \sim \lambda^{-1}$). Evaluating (A8) for (A11) yields an exponential kernel

$$K(t) = g^2 e^{-\tilde{\lambda}t} \Theta(t), \quad g = \sqrt{\frac{\gamma\lambda}{2}}, \quad \tilde{\lambda} = \lambda - i\omega_0, \quad (\text{A12})$$

where $\Theta(t)$ is the Heaviside function. Because $K(t)$ is exponential, the convolutions in Eqs. (A9)–(A10) can be made time-local by introducing two auxiliary amplitudes

$$\begin{aligned} \beta(t) &= ig \int_0^t d\tau e^{-\tilde{\lambda}(t-\tau)} s(\tau), \\ \alpha(t) &= ig \int_0^t d\tau e^{-\tilde{\lambda}(t-\tau)} a(\tau). \end{aligned} \quad (\text{A13})$$

So, the dynamics become an exact closed set of first-

order ODEs for the four amplitudes $(s(t), a(t), \beta(t), \alpha(t))$:

$$\begin{aligned} \dot{s}(t) &= -i(\omega_0 + J) s(t) \\ &\quad + 2ig \cos^2(k_0 d) \beta(t) - g \sin(2k_0 d) \alpha(t) \end{aligned} \quad (\text{A14})$$

$$\begin{aligned} \dot{a}(t) &= -i(\omega_0 - J) a(t) \\ &\quad + 2ig \sin^2(k_0 d) \alpha(t) + g \sin(2k_0 d) \beta(t) \end{aligned} \quad (\text{A15})$$

$$\dot{\beta}(t) = ig s(t) - \tilde{\lambda} \beta(t), \quad (\text{A16})$$

$$\dot{\alpha}(t) = ig a(t) - \tilde{\lambda} \alpha(t). \quad (\text{A17})$$

with initial conditions

$$s(0) = \frac{1}{\sqrt{2}}, \quad a(0) = \frac{1}{\sqrt{2}}, \quad \beta(0) = 0, \quad \alpha(0) = 0. \quad (\text{A18})$$

The exact equations (A14)–(A17) can be written in compact vector form. Define the state vector

$$\mathbf{X}(t) = \begin{pmatrix} s(t) \\ a(t) \\ \beta(t) \\ \alpha(t) \end{pmatrix}, \quad \mathbf{X}(0) = \begin{pmatrix} \frac{1}{\sqrt{2}} \\ \frac{1}{\sqrt{2}} \\ 0 \\ 0 \end{pmatrix}. \quad (\text{A19})$$

Then the dynamics are governed by the linear first-order system

$$\dot{\mathbf{X}}(t) = M(d) \mathbf{X}(t), \quad (\text{A20})$$

where the distance-dependent evolution matrix is

$$M(d) = \begin{pmatrix} -i(\omega_0 + J) & 0 & 2ig \cos^2(k_0 d) & -g \sin(2k_0 d) \\ 0 & -i(\omega_0 - J) & g \sin(2k_0 d) & 2ig \sin^2(k_0 d) \\ ig & 0 & -\tilde{\lambda} & 0 \\ 0 & ig & 0 & -\tilde{\lambda} \end{pmatrix}, \quad (\text{A21})$$

a. Formal solution. Because Eq. (A20) is linear and time-independent, its formal solution is

$$\mathbf{X}(t) = e^{M(d)t} \mathbf{X}(0), \quad (\text{A22})$$

where the matrix exponential is defined by the convergent series

$$e^{M(d)t} = \sum_{n=0}^{\infty} \frac{[M(d)t]^n}{n!}. \quad (\text{A23})$$

b. Eigenmode decomposition. If $M(d)$ is diagonalizable, it admits the similarity decomposition

$$M(d) = P(d) \Lambda(d) P^{-1}(d), \quad (\text{A24})$$

where

$$\Lambda(d) = \text{diag}(\mu_1, \mu_2, \mu_3, \mu_4) \quad (\text{A25})$$

contains the complex eigenvalues $\mu_i(d)$ and the columns of $P(d)$ are the corresponding eigenvectors.

The formal solution then becomes

$$\mathbf{X}(t) = P(d) e^{\Lambda(d)t} P^{-1}(d) \mathbf{X}(0), \quad (\text{A26})$$

or equivalently

$$\mathbf{X}(t) = \sum_{i=1}^4 c_i \mathbf{v}_i e^{\mu_i t}, \quad (\text{A27})$$

where

$$c_i = [P^{-1}(d) \mathbf{X}(0)]_i \quad (\text{A28})$$

and \mathbf{v}_i are the eigenvectors of $M(d)$.

So, using the eigenmode expansion (A27), one obtains the explicit general solution

$$\alpha_1(t) = \frac{1}{\sqrt{2}} \sum_{i=1}^4 c_i (v_{i,s} + v_{i,a}) e^{\mu_i t}, \quad (\text{A29})$$

$$\alpha_2(t) = \frac{1}{\sqrt{2}} \sum_{i=1}^4 c_i (v_{i,s} - v_{i,a}) e^{\mu_i t}, \quad (\text{A30})$$

where $v_{i,s}$ and $v_{i,a}$ denote the symmetric and antisymmetric components of eigenvector \mathbf{v}_i .